JOM, Vol. 68, No. 3, 2016
DOI: 10.1007/s11837-015-1781-1

Spark Plasma Sintering of Aluminum-Magnesium-Matrix Composites with Boron Carbide and Tungsten Nano-powder Inclusions: Modeling and Experimentation

E.S. DVILIS,[1] O.L. KHASANOV,[1] V.N. GULBIN,[2] M.S. PETYUKEVICH,[1] A.O. KHASANOV,[1] and E.A. OLEVSKY[1,3,4]

1.—National Research Tomsk Polytechnic University, Tomsk, Russian Federation. 2.—National University of Science and Technology MISIS, Moscow, Russian Federation. 3.—San Diego State University, San Diego, CA, USA. 4.—e-mail: eolevsky@mail.sdsu.edu

Spark-plasma sintering (SPS) is used to fabricate fully-dense metal–matrix (Al/Mg) composites containing hard ceramic (boron carbide) and refractory metal (tungsten) inclusions. The study objectives include the modeling (and its experimental verification) of the process of the consolidation of the composites consisted of aluminum-magnesium alloy AMg6 (65 wt.%), B_4C powder (15 wt.%), and W nano-powder (20 wt.%), as well as the optimization of the composite content and of the SPS conditions to achieve higher density. Discrete element modeling of the composite particles packing based on the particle size distribution functions of real powders is utilized for the determination of the powder compositions rendering maximum mixture packing densities. Two models: a power-law creep model of the high temperature deformation of powder materials, and an empirical logarithmic pressure–temperature–relative density relationship are successfully applied for the description of the densification of the aluminum-magnesium metal matrix powder composite subjected to spark-plasma sintering. The elastoplastic properties of the sintered composite samples are assessed by nanoindentation.

INTRODUCTION

The development of nuclear energy applications, space exploration, and the use of radiation in medicine depends on the solution of various problems of the protection of structural materials, electronic components and products, and biological tissues from their exposure to ionizing radiation. Therefore, the design and development of new materials to improve the effectiveness of anti-radiation protection is an important modern area of research. It includes the reduction of the weight and dimensions of radiation-shielding materials.

Light metal alloys have good mechanical properties, but when subjected to radiation, they are susceptible to swelling and structural changes. These defects can be prevented by creating metal–matrix composites containing particulate fillers with the required radiation-shielding properties. The use of radiation-absorbing nanoparticles of heavy metals and ceramic materials as fillers dispersed within metal–matrix composites improves these composites' absorption properties with respect to the neutron, gamma and x-rays.[1,2]

In Ref. 3 it is shown that the use of Al/Mg matrix filled with nano-scale particles of radiation-absorbing ceramic and metallic materials (e.g., B_4C and W) increases the neutron absorption factor at least 2 times and the gamma radiation scattering coefficient by 28–73%.

To manufacture composite materials of similar kinds, various approaches have been used.[4,5] In particular, the method of hot extrusion has been applied.[3] The composite material included 60–65 wt.% of aluminum-magnesium alloy (grades AMg6 or V95), 15–20 wt.% of W nano-powder, and B_4C (or BN), the rest. Mixing of initial powders was carried out by planetary ball milling, and then the vacuum degassing by heating was performed. The hot extrusion of the powder mixture has been conducted in special aluminum shells at temperatures of $(0.8–0.9)T_{melt}$ of AMg6 (or V95) to shape the

(Published online January 19, 2016)

1000 × 50 × 10 mm components. The extrusion of the composites occurred without phase transformations but resulted in the formation of the material of 95% relative density only.[3]

In the present work, we applied the spark-plasma sintering (SPS) technique to sinter similar metal–matrix (Al/Mg) fully-dense composites containing hard ceramic (B_4C) and refractory metal (W) inclusions. SPS and related field-assisted sintering technologies[6] have previously been successfully used to consolidate hard-to-deform ceramic,[7–9] metal,[10] and composite[2,11] powder systems.

Another possible venue for processing composites of this kind is liquid phase sintering. To use liquid phase sintering, however, it is necessary to ensure the sufficient wetting of the particles of the composite including the nanoparticles, whose specific surface area is very high. Therefore, this method of fabrication is difficult to implement; it should involve multiple stages and requires the application of external pressure. It is also possible to melt the AMg6 matrix during the SPS process; however, this causes higher energy consumption, and may also lead to an unstable state of the sample, when even under slight pressure the molten matrix phase will flow into the gaps of the SPS tooling (spaces between punches and dies), causing changes in the component concentrations of the composite material system.

The present work objectives include the modeling (and its experimental verification) of the process of the consolidation of the composites consisted of aluminum-magnesium alloy AMg6 (65 wt.%), B_4C powder (15 wt.%) and W nano-powder (20 wt.%), as well as the optimization of the composite content and of the SPS conditions to achieve higher density.

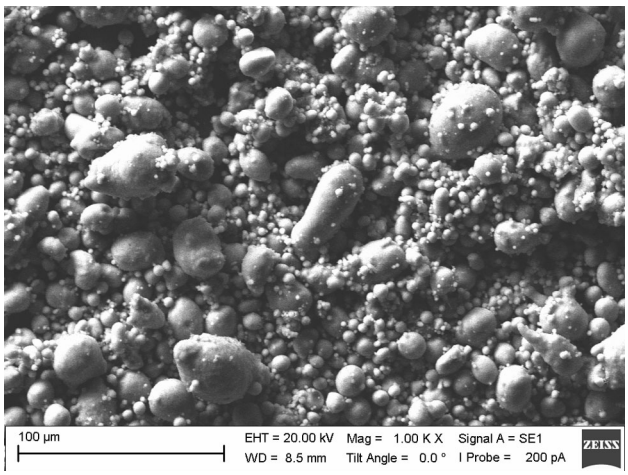

Fig. 1. AMg6 matrix alloy powder obtained by scanning electron microscopy.

USED POWDER MATERIALS AND EXPERIMENTAL PROCEDURES

The characterization of initial powders and their mixtures has been performed by scanning electron microscopy (SEM) and energy dispersive spectroscopy (EDS) analysis (JSM-7500F, JEOL; LEO EVO 50, Zeiss), x-ray diffraction (XRD) analysis (XRD-7000S, Shimadzu), particle size distribution analysis using laser diffraction technique (SALD-7101, Shimadzu), and specific surface analysis by Brunauer, Emmett and Teller (BET) method (Sorbi META).

The powders were mixed by ball milling in a roller mill using zirconia milling balls. The densification behavior of the dry mixed composite powder has been analyzed using a computer-controlled hydraulic precision press (IP-500 M-auto, ZIPO). The consolidation of the mixed composite powder was conducted using pressureless sintering in a vacuum furnace (VHT 8/22GR, Nabertherm), and by SPS technique (SPS 515S, SYNTEX). The sizes of green samples were 15 mm in diameter and 3–6 mm in height.

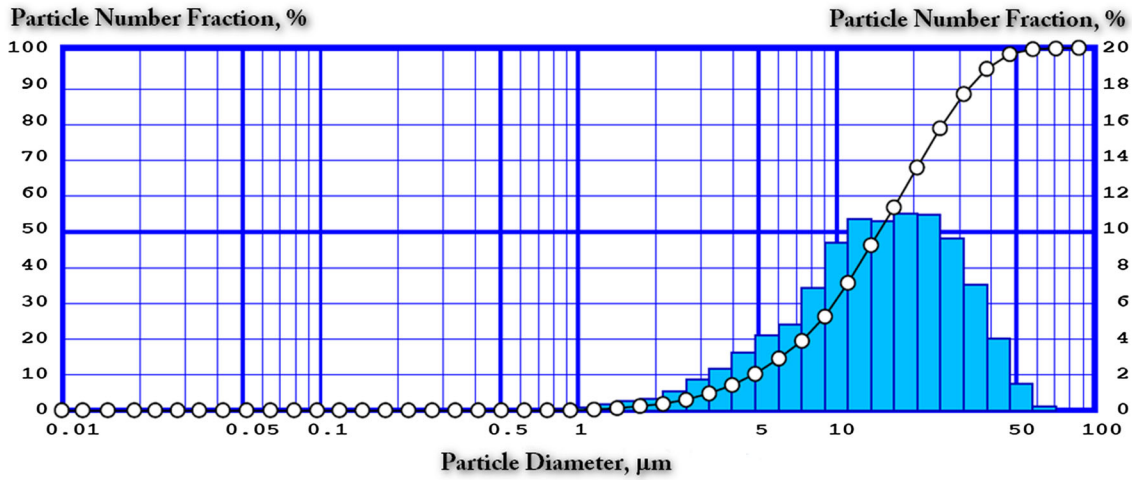

Fig. 2. Size distribution of AMg6 matrix alloy powder obtained by laser diffraction analysis.

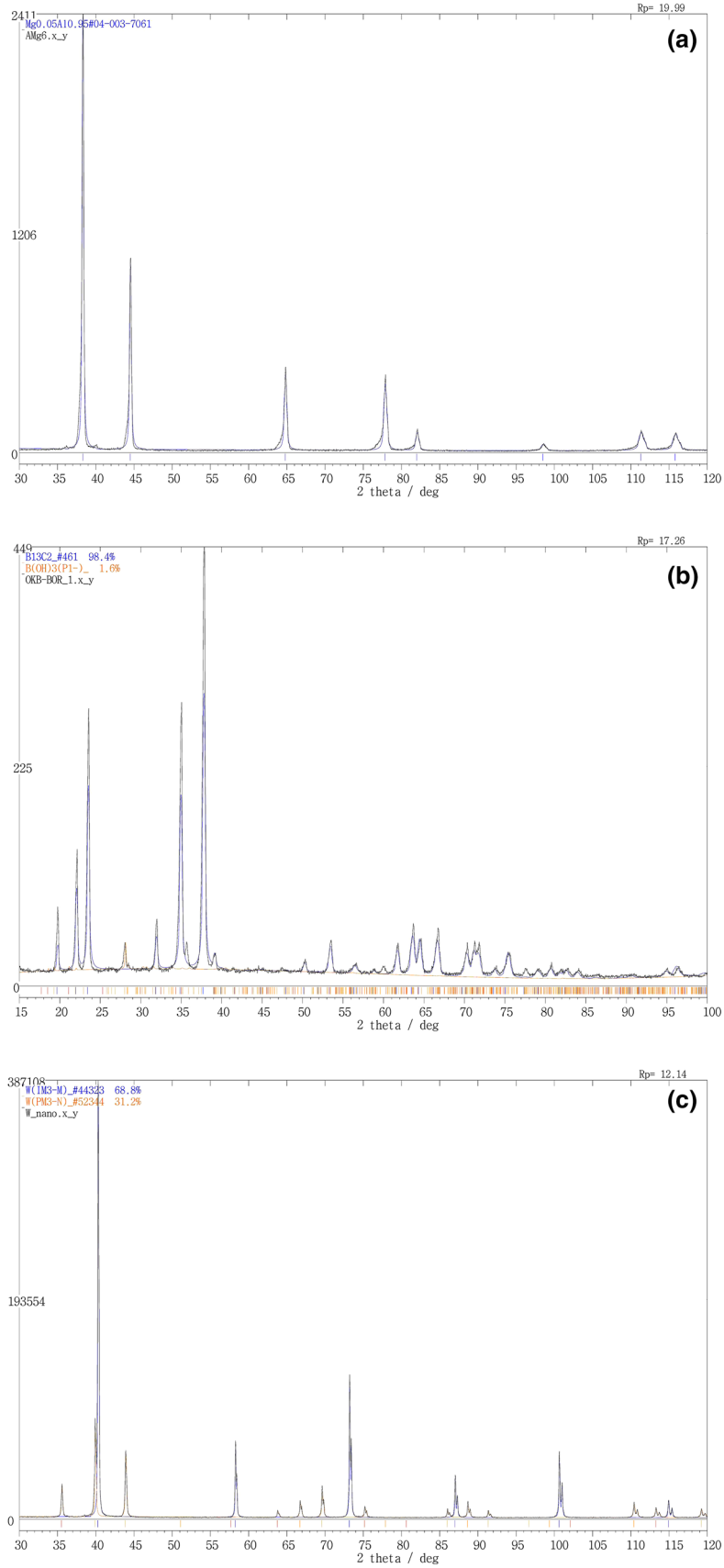

Fig. 3. XRD patterns of the utilized powder materials: (a) AMg6 matrix alloy powder; (b) boron carbide powder; (c) tungsten powder.

Table I. Average particle/agglomerate sizes of the components in the powder mixture

Component	Average size (micron) of structural elements according to different analysis				
	XRD (crystallite size)	SEM (agglomerate size)	Laser diffraction (agglomerate size)	BET (particle size d_m)	Agglo-meration degree
AMg6	0.2	15.4	13.6	6.8	2
B_4C	0.043	1.8	1.22	0.275	4.43
W	0.093	1.1	1.07	0.115	9.3

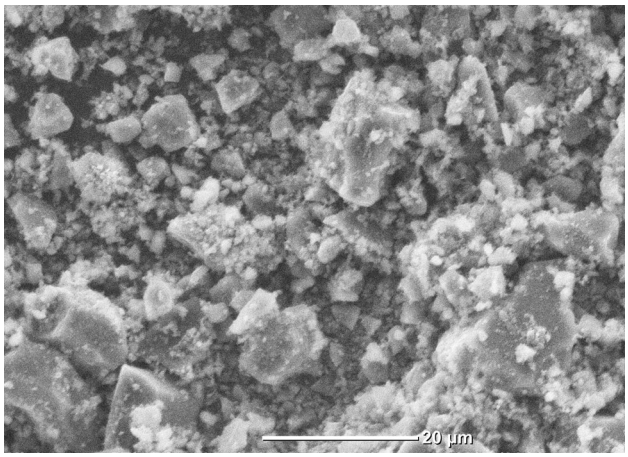

Fig. 4. Boron carbide powder obtained by scanning electron microscopy.

The mechanical properties of the consolidated specimens were determined by nanoindentation (DUH 211S, Shimadzu) of the polished surfaces of sintered samples.

AMg6 powder The commercial magnesium aluminum alloy powder AMg6 (AA5556 alloy analogue) consists of particles with a shape close to spherical (Fig. 1), with a wide (up to 2 orders of magnitude) spread in particle sizes (Fig. 2). The AMg6 composition is (in wt.%): Fe: 0.4, Si: 0.4, Mn: 0.5–0.8, Ti: 0.02–0.1, Al: 91.1–93.68, Cu: 0.1, Be: 0.0002–0.05, Mg: 5.8–6.8, Zn: 0.2.)

The results of the XRD analysis of all the three used powder materials are shown in Fig. 3a–c. The conducted XRD and EDS analyzes of the AMg6 powder indicate less than 2% impurities. The broadening of the XRD reflexes confirms the presence of submicron fractions in the powder (Fig. 3a). The degree of agglomeration of the powders has been assessed in terms of the ratio of the mean particle size obtained by the laser diffraction method and the average particle size obtained by the BET method. AMg6 powder agglomeration degree is equal to 2 (Table I), i.e., this powder was weakly agglomerated.

B_4C powder The commercial boron carbide powder produced by "OKB-BOR" (Russia) has a nearly equiaxed particle shape (Fig. 4) with a wide (up to 2 orders of magnitude) spread in particle sizes (Fig. 5). The conducted XRD and EDS analyses did not reveal any impurities in the powder (Fig. 3b). The B_4C powder agglomeration degree is equal to 4.43 (Table I). This indicates the presence of up to 10% of a fraction of nano-particles (Fig. 5).

W powder Tungsten powder was prepared by electric explosion of tungsten wire.[12] The powder particles have a spherical shape (Fig. 6) and wide (over 2 orders of magnitude) multimodal size distribution (Fig. 7). The powder contains 20% nano-sized (80–200 nm) and 20% submicron (200–900 nm) fractions, and therefore the degree of agglomeration of the W powder is 9.3 (see Table I). The powder consists of the two modifications of cubic tungsten: with lattice parameters a = 3.1656 Å (IM3-M) and a = 5.0521 Å (PM3-N) (Fig. 3c); no impurities in the tungsten powder were detected.

The summary of the dimensional characteristics of the starting powders is provided in Table I. The analysis of the obtained data indicates that the initial raw powders have a fairly wide particle size distribution, but their mixture can be optimized with respect to the concentration of the components to form a continuous alloy matrix and to increase the packing density of the particulate filler. Given the morphological characteristics of the powders, the maximum density of packing can be expected when filling the space between tightly packed particles of the matrix alloy by a mixture of boron carbide particles with tungsten particles' agglomerates. Parameter d_m in Table I has been determined for spherical particles using specific surface value S_{BET} (BET data) and theoretical density ρ, for respective materials:[13]

$$d_m = \frac{6}{\rho S_{BET}} \quad (1)$$

OPTIMIZATION OF POWDER MIXTURES

Nearly spherical and equiaxed particle shape of the used powders enables the modeling of their packing and optimization of their mixing ratio in terms of the values of the average number of inter-particle contacts (the coordination number N_c) and

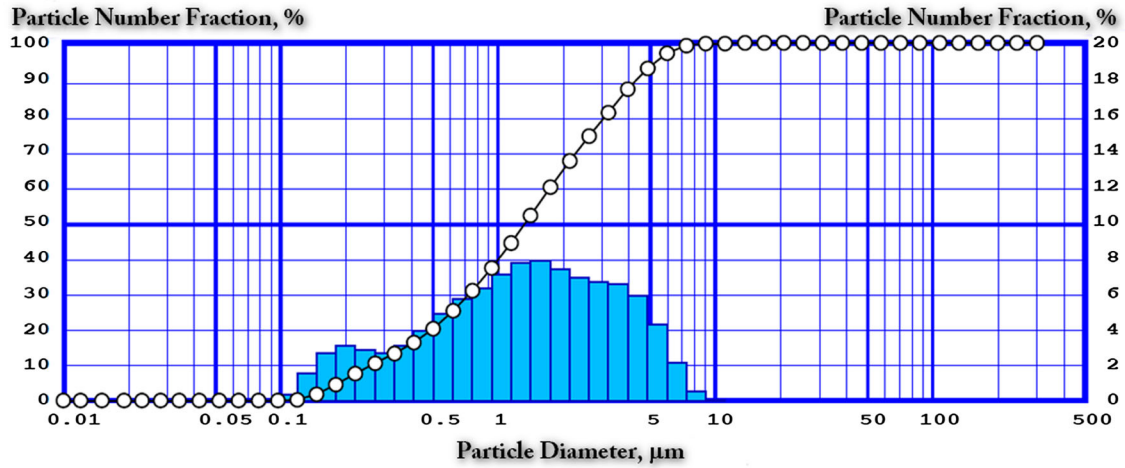

Fig. 5. Size distribution of boron carbide powder obtained by laser diffraction analysis.

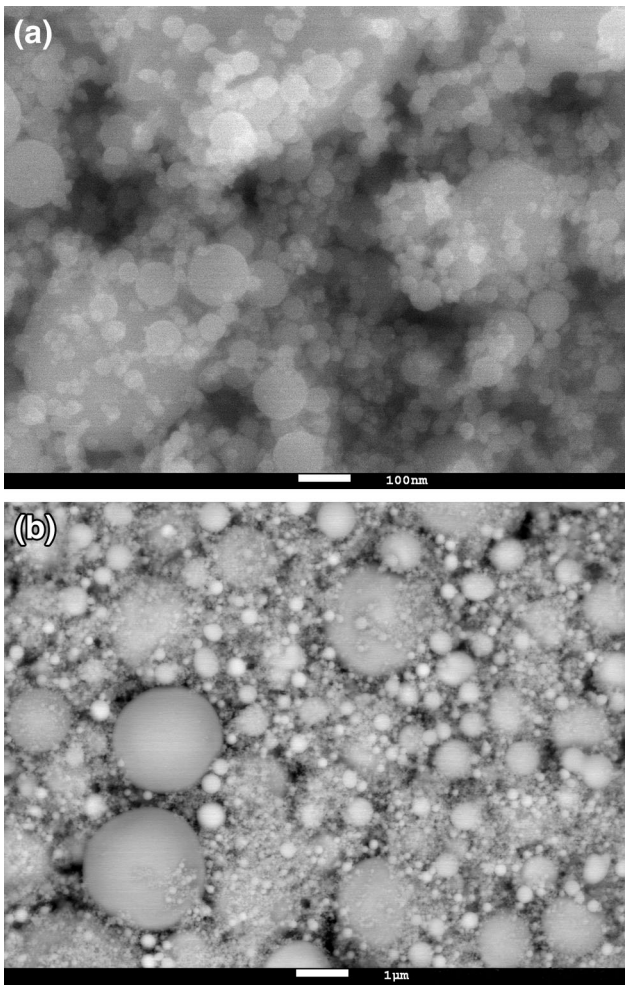

Fig. 6. (a, b) Tungsten powder obtained by scanning electron microscopy: (a) nano-size particles; (b) largest particles.

of the packing density. For this purpose, the particle size distributions obtained by laser diffraction have been approximated by matching functions. These functions were used to define the relevant classes of particles in the framework of the discrete element model environment of the S3D PorouStructure™ software (Smart Imaging Technologies™, TX, USA) utilizing the Ichikawa algorithm (with central packing).[14] The total number of particles in a representative model set (Fig. 8) varied from 20,000 to 72,000.

The comparative analysis of the results of the modeling of the packing of the composite structure AMg6 (65 wt.%) + B_4C (15 wt.%) + W (20 wt.%) was carried out using S3D Evolution™ code (Smart Imaging Technologies™). For this simulation, the compaction parameters were associated with the deformation of the particles of the matrix alloy and tungsten, subjected to pressures from 40 MPa to 800 MPa (including at temperatures up to 600°C). The particles of boron carbide were considered to be non-deformable (Fig. 8b and d).

The conducted packing's statistical analysis based on the criteria of the maximum density and of the ensured continuous contact of the aluminum matrix particles showed the following. The minimum composition forming a contiguous aluminum alloy matrix rendering the optimal dense filling of the dispersed particles of tungsten and boron carbide was found to be 65% AMg6 + 15% B_4C + 20% W (Fig. 8a and b). For such a mixture in the initial underformed packing state, the alloy particles' average partial coordination number (the number of contacts between alloy particles only, excluding tungsten and boron carbide particles) is in the range of the minimum allowable values ($1 < N_c < 2$), and the space between them can be filled by the optimal content of tungsten and boron carbide particles with a predetermined size distribution. However, the mixing ratio rendering the maximum packing density of the particles has a different composition: 74% AMg6 + 6% B_4C + 20% W (Fig. 8c and d). For this composition, the partial coordination number of the matrix alloy particles ranges from 3 (in a loose powder state) to 4 (after plastic deformation of the

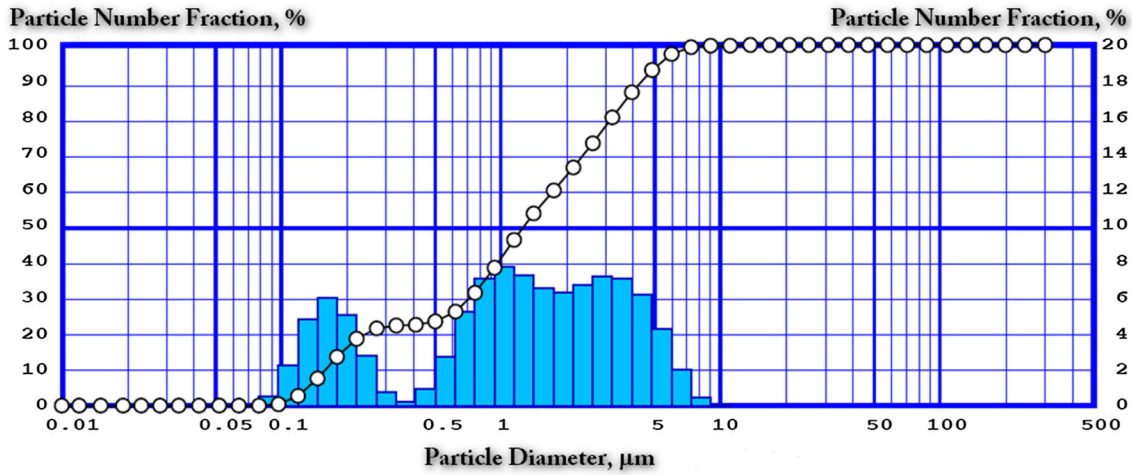

Fig. 7. Size distribution of tungsten powder obtained by laser diffraction analysis.

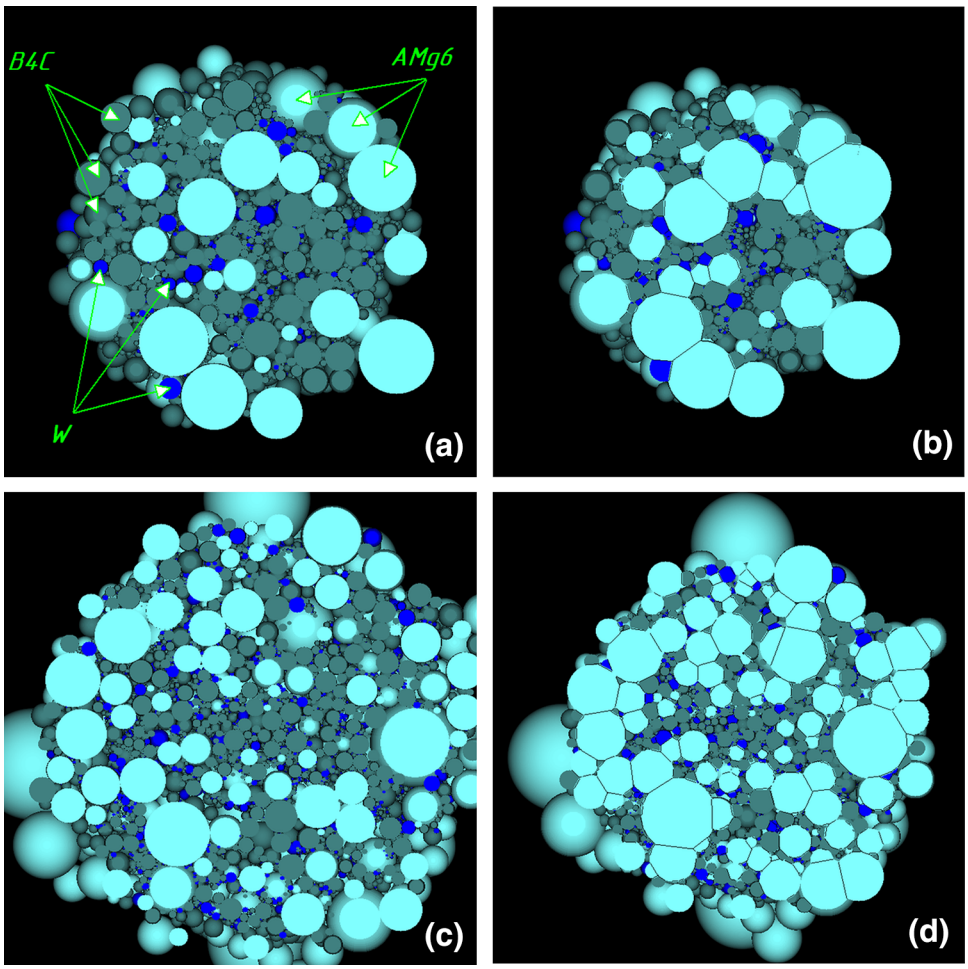

Fig. 8. (a–d) Models of packing for the composites with minimum permissible (a, b) and the optimal density of the matrix alloy and particulate fillers, (c, d) in a free-laying state (a, c) and after plastic deformation of the particles (b, d): AMg6 particles blue; B_4C gray; W dark blue (Color figure online).

particles), and the partial density of the alloy particle packing varies from 43% (Fig. 8c) to 67% (Fig. 8d), respectively.

The quantitative results of the modeling for the two above-mentioned mixtures are presented in Table II, from which it follows that the increase in the partial

Table II. Parameters of deformed packed structures of composite's particles

Characteristics of composite with optimal particles density packing and minimum possible content of the matrix alloy (after deformation 25%)

Component [theoretical density (g/cm^3)]	Content (%)		Partial packing density	Average coordination number for the component particles	Partial coordination number for particles in the powder component
	wt.%	vol.%			
AMg6 (2.6)	65	77.9	0.276	95.04	1.78
B_4C (2.52)	15	18.8	0.498	6.23	4.42
W (19.25)	20	3.3	0.057	5.17	0.83
Mixture (3.14)	100		0.782	6.49	6.49
AMg6 (2.6)	74	89.2	0.67	124.7	4.29
B_4C (2.52)	6	7.5	0.254	6.34	3.28
W (19.25)	20	3.3	0.052	5.23	1.54
Mixture (3.14)	100		0.89	7.23	7.53

coordination number from 1.78 to 4.29 in a continuous AMg6 matrix can be achieved by increasing the content of the powder alloy by 9 wt.% (from 65% to 74%). In this case, the strength of the composite can be increased by at least 2.5 times, assuming that the matrix material is the only component in the consolidated mixture capable of bearing mechanical load, and the strength of the porous material is directly proportional to its density. An improvement of the strength of such a composite is also possible when using a fine powder of boron carbide which would effectively fill the space between the densely packed particles of the matrix alloy.

ANALYSIS OF COMPOSITE MATERIAL CONSOLIDATION

Consolidation efficiency studies were carried out for the powder mixture composition including aluminum-magnesium alloy AMg6 (65 wt.%), B_4C powder (15 wt.%) and W nano-powder (20 wt.%).

The conducted analysis of the powder packing (Fig. 8; Table II) indicates that such a composite structure cannot be consolidated by free solid state sintering. Without the application of pressure and in the absence of a liquid phase, the contiguous AMg6 matrix is not formed in this composite, and filler particles prevent the alloy particles' junction. After pressure-assisted packing of the particulate mixture, its further consolidation decreasing the free surface at temperatures below the melting point of the AMg6 alloy (T_m = 600°C) is limited by the presence of densely packed particles of boron carbide and tungsten in the matrix inter-particle space, which require much higher sintering temperatures. The densification of the composite at temperatures near 600°C is only possible by plastic deformation, and by the forced flow of the matrix material (intrusion) into the pore spaces within the particulate filler, until all the pores are filled.

Therefore, pressing is the main process for the effective consolidation of the tested composites, and thermal effects should be considered to be an additional deformation-resistance-reducing factor influencing the constitutive properties of the matrix material. Thus, the study of the consolidation of the aluminum-matrix composites containing dispersed filler particles of boron carbide and tungsten is reduced to the study of their density dependence on the applied pressure for different temperature-affected constitutive properties of the matrix material.

Due to the composite structure of the tested material with considerably different deformational mechanisms of its phases, in general, it should exhibit more complex densification behavior than homogeneous porous materials. The degree of the deformation of this composite, for given processing settings may not evolve significantly under stationary conditions, and further densification may be able to proceed only by increasing pressure or temperature.

These possible specifics of the studied powder composite's constitutive behavior are confirmed by the analysis of the typical microstructure of a composite sintered by SPS (Fig. 9a). One can observe substantially separate grains of the aluminum-magnesium matrix alloy; their mutual sintering is limited by the presence of the particulate filler refractory particles' agglomerates, whose intrusion into the inter-particle pores of the aluminum-magnesium matrix can occur only under pressure and provided a significant reduction in the deformational resistance of the matrix due to the elevated temperature influence.

It should be noted that both the achievement of the high degree of densification and the properties of inclusion–matrix interfaces are some of the major factors influencing the mechanical properties of metal matrix powder composites. Figure 9a indicates that the efficient densification (up to a practically full density state) of the studied composites has been successfully carried out. Table III shows that the achievement of the almost fully-dense state also results in a substantial increase of hardness

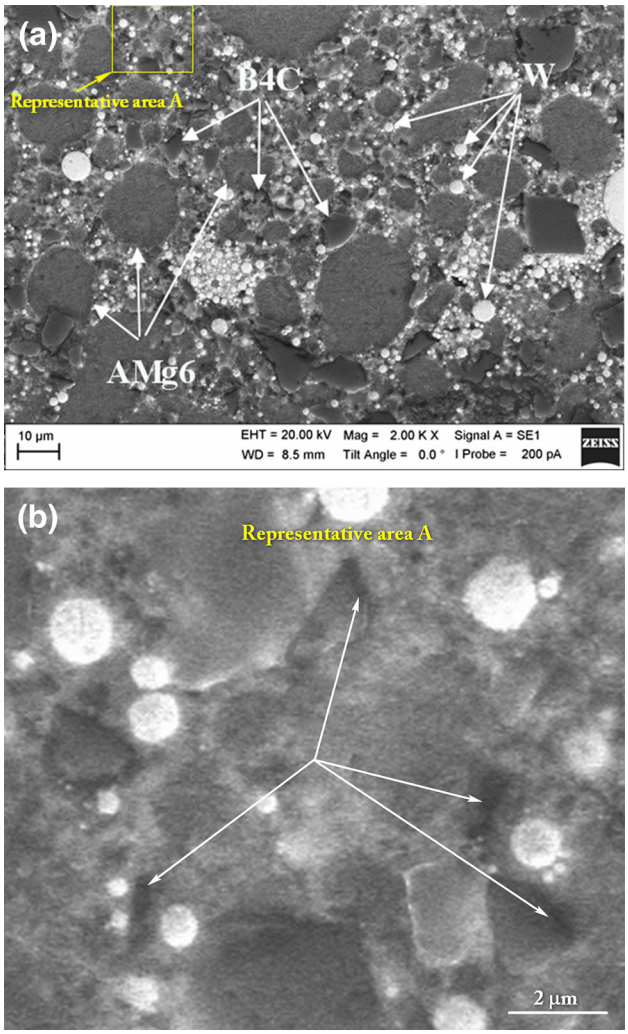

Fig. 9. (a) Microstructure of the composite material consolidated by SPS at 490°C under 39 MPa of applied pressure. (b) Representative microstructure of the composite material consolidated by SPS showing limited number of pores of neither spherical, no equiaxial (isomeric) shape.

and of elastic properties of the fabricated composites. In addition, the obtained microscopic evidence, such as the one shown in Fig. 9a, indicates another important outcome of the processing: the uniformity of the spatial distribution of the powder system component phases.

The properties of the inclusion–matrix interfaces are usually directly revealed during specimen microscopic characterization, when after a respective probe preparation (cutting, grinding and polishing) some of the inclusions with weak interfaces are removed from their respective "nest" areas, creating the specific for these material systems "cavity-filled" morphology. A careful examination of only a few available pores (Fig. 9b) shows that they are neither spherical nor equiaxial (isomeric) in shape. This fact indicates that these cavities could not be created by the de-cohesion of W inclusions (since W inclusions have a close to ideal spherical shape), nor by the de-cohesion of B_4C inclusions (since B_4C inclusions have a close to equiaxial shape). Thus, the origin of these few pores is apparently related to some initial localized packing non-uniformities. Thereby, Fig. 9b (as well as the data in Table III) can be considered to be an indirect indication of the relatively high strength of the inclusion–matrix interfaces.

Conventional Quasi-Static Pressing of the Powder Composite

The powder compressibility characterization has been performed by plotting the compaction curves $\rho(P)$ obtained for the conditions of uniaxial quasi-static pressing with loading–reloading cycles and using an approximation by a logarithmic equation in a dimensionless form:[15,16]

$$\rho = b \cdot \ln\left(\frac{P}{P_{cr}}\right) + 1 \qquad (2)$$

where ρ is the relative density of the green body; P is the applied compaction pressure; P_{cr} is the critical pressure (pressure enabling compaction up to full density of the powder material); and b is a material constant defining densification pressure sensitivity. Due to the limitations on the values of the relative density ($0 < \rho \leq 1$), Eq. 2 is valid for a limited range of the values of the applied pressure: $\frac{P_{cr}}{\exp(1/b)} < P \leq P_{cr}$.

The results presented in Fig. 10 (with approximation certainty not less than 99.9%) show that, for the conventional quasi-static pressing in a rigid die, the critical pressure value P_{cr} for the tested composite is 5.219 GPa, which exceeds the strength limit of hardened steel, the structural material of the pressing die. While the AMg6 alloy powder without a particulate filler may be densified at low temperatures down to a non-porous state under the critical pressure of 1.262 GPa using a special tungsten carbide die of the collector type,[16] the achievement of the critical pressure of 5.219 GPa for pressing bulk components of complex shapes made of the studied composite material appears to be impossible.

At pressure of 750 MPa the composite powder (65% AMg6 + 15% B_4C + 20% W) samples with a density of 85.3% were obtained by the conventional cold quasi-static pressing. During free sintering of these samples in a vacuum at temperatures of 450°C, 500°C, 550°C and 600°C, the linear dimensions of the processed specimens remained unchanged up to the melting point of the aluminum-magnesium matrix. This fact indicates a non-significant contribution of the pressureless solid-state diffusion-based mass transport into the densification of the studied powder composites.

Table III. Elastic-plastic properties of the composite samples sintered by SPS

T (°C)	t (min)	ρ (%)	E_{it} (N/mm^2)	C_{it} (%)	n_{it} (%)	HV
440	5	86.1	50460	1.07	13.1	129.9
490	5	97	78960	1.12	13.9	287.5
440	10	90.1	56295	1.53	14.8	148.3
490	10	100	98620	1.45	22.4	419.9

T maximum SPS temperature, *pre-compaction pressure* P = 39 MPa, t SPS dwell time, ρ relative density, E_{it} Young modulus obtained by nanoindentation, C_{it} creep strain at constant indentation load, n_{it} fraction of the material elastic deformation at nanoindentation, *HV* Vickers microhardness.

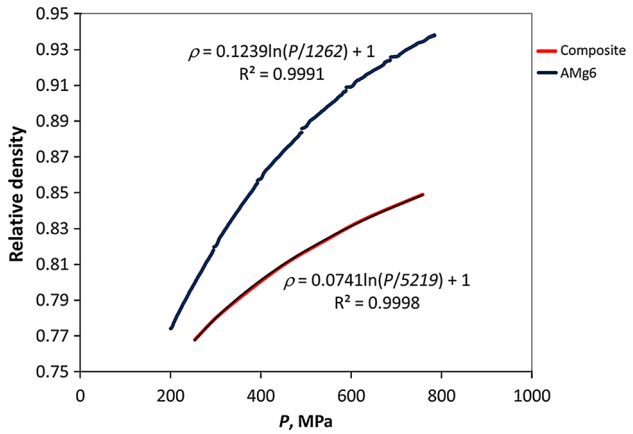

Fig. 10. Pressure–density dependence for AMg6 matrix alloy and composite (65%AMg6 + 15%B_4C + 20%W) powders compacted by conventional quasi-static pressing in a rigid die.

For the powder with an optimized composition (74% AMg6 + 6% B_4C + 20% W) subjected to the quasi-static pressing at the same pressure of 750 MPa, a density of 91.6% has been achieved, which confirms the results of the simulation-based optimization of powder mixtures (Fig. 8c and d; Table II).

It should be noted that for the tested composite the conventional quasi-static pressing may also be applied in the case of the yield strength reduction of the AMg6 alloy even under ambient temperature conditions. One can use a well-known acoustic-plastic effect by utilizing powerful ultrasonication during materials compression, which can significantly increase the concentration and mobility of dislocations of the crystal lattice of the matrix material, thereby reducing its yield strength. In particular, according to Ref. 17, the effect of ultrasound on the deformation process of aluminum at an oscillating stress amplitude of 0.2 kg/mm^2 (~1.9 MPa) and under static loading of 1 kg/mm^2 (~9.8 MPa) increases the steady creep rate almost 10-fold, and the yield strength decreases by half.

Additional effects can be achieved by using carbide materials for the collector-type dies, which enable the achievement of the pressure levels higher than the tensile strength of the material of such dies.[16]

In the present work, Eq. 2 will be utilized, not only for the description of the plastic deformation of the AMg6 matrix alloy but also as one of the possible models for the analysis of the consolidation of the studied composite material, containing boron carbide particles, which are essentially non-deformable in the specified pressure range (see next section).

High-Temperature Consolidation: Modeling and Experiment

To describe the high-temperature consolidation of the studied composite, a numerical solution of the porosity evolution equation is utilized in the present work. For this purpose, the continuum theory of sintering capable of modeling high-temperature creep of powder and porous materials under external mechanical action is employed[18,19] (hereinafter—Model 1). According to this model, the rate of change of the porosity of a powder body ($d\theta/dt$) during hot pressing in a rigid die depends upon the specimen's material current structure (porosity θ), temperature T, axial pressure P, and empirical constants: the power law creep pre-exponential factor at a given temperature A_m (MPa/K^m), the creep activation energy Q (kJ/mol) and the dimensionless strain rate sensitivity m:

$$\frac{d\theta}{dt} = -\left(\frac{P}{A_m \cdot T^m \cdot \exp\left(\frac{m \cdot Q}{R \cdot T}\right)}\right)^{\frac{1}{m}} \cdot \left(\frac{3\theta}{2}\right)^{\frac{m+1}{2m}} \cdot (1-\theta)^{\frac{m-3}{2m}} \quad (3)$$

The material constants in Eq. 3 have been determined by the method of least squares on the basis of the numerical finite-difference inverse regression of the experimental data.

An experimental high-temperature composite consolidation was carried out by spark-plasma sintering. To verify the consolidation simulation results, the time evolution of the main parameters of the sintered samples: temperature, pressure, and axial shrinkage have been recorded.

The axial relative displacement of the graphite die and punches was monitored with a position sensor imbedded in the SPS device. For each

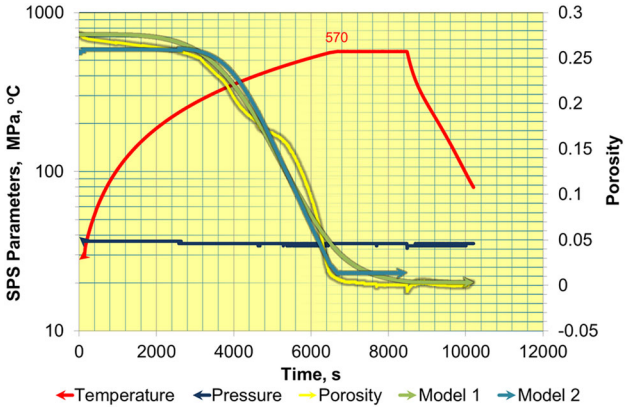

Fig. 11. Experimental and model description of the porosity evolution of the composite material with a monotonic change of SPS temperature of up to 570°C and at constant applied pressure (39 MPa).

experimental case, a control procedure was conducted by employing the tooling setup in the absence of powder and imposing the same experimental conditions. Such a process provided the necessary data to compensate for the expansion and shrinkage of the tooling material. The final porosity of the processed specimens has been determined by the Archimedes method; then the respective porosity evolution has been backwards-calculated using the known final porosity value, the axial relative displacement data, and taking into account the above-mentioned measured thermal expansion and contraction of the SPS tooling. All the reported tests have been repeated twice and indicated not more than 1% difference in the experimental outcomes (with thereby insignificant uncertainty levels).

The results of the numerical solution of Eq. 3 can adequately describe the densification kinetics of the powder material in the process of SPS. Figure 11 is a diagram of the composite material's porosity evolution under gradual change in temperature of the SPS process and constant applied pressure. The experimental data are represented, taking into account the changes in the volume of the powder sample due to thermal expansion and elastic deformation of the powder material and SPS tooling.

The results of the inverse experimental data regression analysis of the constitutive parameters of the power law creep in accord with Model 1 indicate that the major pore closure mechanism is based on the combination of dislocation climb and glide (when strain rate sensitivity m is indicated to be in the range of 0.3–0.35).[8] Dislocation climb is a rather typical mass transport mechanism for conventional hot pressing of metal powders, while dislocation glide is usually associated with the rigid-plastic behavior of powder and porous materials under conditions of cold pressing. For the studied composite, the main contributor to the plastic flow decreasing the overall porosity is the AMg6 matrix phase with a possible minor contribution of W particles. The boron carbide particles behave like rigid inclusions, which in some cases may move inside the adjacent available pore spaces, thereby contributing to filling some portion of the pore volume.

The applied model (Model 1) provides a minimal (1.5%) deviation of the estimated porosity of the sample from the experimental values within the porosity change from 27.6% to 0%. The bend in the experimental porosity curve at 5000 s (Fig. 11) may be caused by local melting. However, the rapid step-wise changes in the conditions of the material processing (temperature and pressure) can be taken into account only by partitioning the experimental curve into portions, with each of the portions having its own material parameters utilized in Eq. 3. The latter fact may be the evidence of the change of the SPS dominant mass transport mechanisms due to the rapid change of the processing conditions.

Figure 12 shows the results of an experiment with a step-wise change in the SPS parameters: temperature (100°C, 350°C, 400°C), pressure (17 MPa, 24 MPa, 29 MPa, 39 MPa). The resulting step-wise porosity kinetics is described by Model 1 with a substantial discrepancy, provided that the same values of the material constants are employed as those used for the approximation of the experimental data shown in Fig. 11. The reason (aside from the possible influence of SPS-specific thermal and field factors[20–23]) is that the analyzed composite material exhibits much lower strain rate sensitivity in the temperature range below 500°C, thereby manifesting properties more typical for a conventional cold quasi-static pressing. In this case, the porosity of the material is rapidly changing with changing pressure or temperature, but it is weakly dependent on the time of sintering at constant pressure and temperature conditions. Thus, a further substantial densification is possible mostly due to the increase in pressure or changes in the constitutive properties of the material at higher temperatures.

A better approximation of these low-temperature SPS experimental data can be achieved in the framework of Model 1 by decreasing the value of the strain rate sensitivity m in Eq. 3. Indeed, the values of m approaching zero correspond to the rigid-plastic behavior of powder materials characteristic for the conditions of cold pressing. At the same time, the low rate sensitivity opens the possibility of the direct usage of the pressure–density relationship (2). In fact, Eq. 2 provides an "instantaneous" link between the applied pressure and the achieved level of the relative density, which does not involve any time dependence and, therefore, is suitable for the description of rigid-plastic response of powder materials.[18]

Assuming that the minimum resistance to deformation can be achieved at some reference temperature T_m, Eq. 2 should be supplemented by a term rendering the dependence on the magnitude of the current relative temperature (T/T_m) with a power constant n, which characterizes the rate of change of the relative density with increasing temperature:

$$\rho = b \cdot \ln\left(\frac{P}{P_{cr}} + \left(\frac{T}{T_m}\right)^n\right) + 1 \quad (4)$$

or porosity θ:

$$\theta = -b \cdot \ln\left(\frac{P}{P_{cr}} + \left(\frac{T}{T_m}\right)^n\right) \quad (5)$$

The description of the consolidation process of the composite by Eq. 5 (hereinafter Model 2) is in satisfactory agreement with the experimental data obtained at SPS consolidation under monotonic temperature change and under a constant applied pressure (Fig. 11). Obviously, Model 2 is not capable of describing the powder material deformation under a constant mechanical stress and at a constant temperature, and it does not render adequate results for the cooling and unloading stages of the SPS process. However, for an increasing load and temperature, Model 2 well describes the evolution of porosity, even for an arbitrary step-wise change of pressure and temperature (Fig. 12).

Model 2-based results (Fig. 12) have been obtained using the values of the densification pressure sensitivity b = 0.0741 and critical pressure P_{cr} = 437 MPa derived from the densification curves shown in Fig. 12. For Eq. 5, the densification rate with increasing temperature (n = 2,7225) and reference material temperature (T_m = 2070°C) have been obtained by the inverse regression of the empirical data given in Fig. 12.

The results shown in Fig. 12 indicate that this empirical model adequately describes the consolidation of the studied powder composite by the SPS process.

MECHANICAL PROPERTIES OF THE SINTERED COMPOSITES

The composite (65% AMg6 + 15% B_4C + 20% W) was sintered to a density of 100% at the temperature of 490°C, the dwell time of 10 min, and under the applied pressure of 39 MPa (Table III).

The elastoplastic properties of the sintered composite samples have been assessed by nanoindentation using Vickers diamond indentor. The determined values are provided in Table III.

The results show that the final properties of this material are not always unambiguously dependent on the consolidation mode parameters. In particular, a non-monotonic behavior is manifested by the creep strain at constant indentation load, the fraction of the material elastic deformation under nanoindentation and microhardness.

CONCLUSION

The described study combined the experimental and theoretical research on the consolidation of multi-phase metal matrix powder composites including (1) the modeling-based optimization of the pre-consolidation packing densities, (2) the experimental verification of the outcomes of the modeling of powder packing (utilizing the real experimentally measured particle size distributions for each powder phase), (3) the comparative physically-based and empirical modeling of the high-temperature compaction of the optimized powder mixtures, and (4) the experimental verification of the high-temperature compaction modeling.

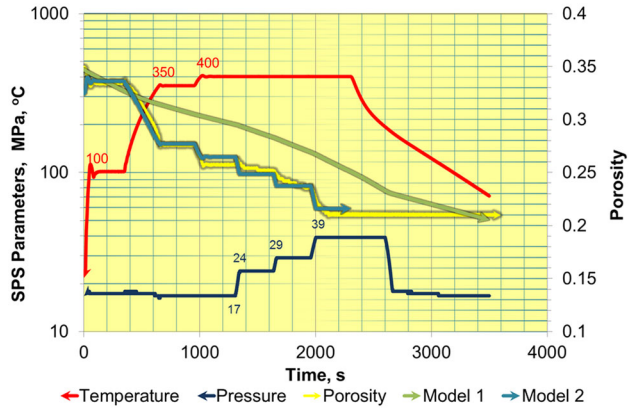

Fig. 12. Experimental and model description of the porosity evolution for the composite material with a non-monotonic variation of SPS modes: temperature (100°C, 350°C, 400°C), applied pressure (17 MPa, 24 MPa, 29 MPa, 39 MPa).

The conducted study led to the following conclusions:

- Discrete element modeling of the composite particles' packing based on the particle size distribution functions of real powders well describes the mixing of the powder components and enables the determination of the powder compositions rendering maximum mixture packing densities.
- The optimal content of the studied composite has been determined (74%AMg6 + 6%B_4C + 20%W). This content provides the maximum dense particle packing for all the components and strong alloy matrix with the coordination number greater than 4 and packing density of 0.67. The experimentally obtained density of this composite material subjected to the conventional quasi-static pressing (under pressure of 750 MPa) was 91.6%.
- Free solid state sintering is not suitable for the consolidation of the 65%AMr6 + 15%B_4C + 20% composite. Spark plasma sintering of this composite material rendered full density specimens.
- The densification during spark plasma sintering of the studied powder mixture mainly occurs during pressure or temperature increase.
- The power-law creep model based on the continuum theory of sintering adequately describes the densification kinetics of the composite material during spark plasma sintering. An advantage of the utilized modeling of densification by spark plasma sintering is in its capacity of using only

in situ macroscopic displacement data to clarify the powder composite deformational mechanisms and to directly obtain the values of the important constitutive parameters, such as the coefficients of power-law creep.

- The logarithmic compaction equation in a dimensionless form including the temperature-sensitive term is suitable for modeling the composite consolidation at non-constant pressure and temperature SPS conditions.
- The final properties of the spark plasma sintered composite material are not always unambiguously dependent on the consolidation mode parameters.

ACKNOWLEDGEMENTS

The work has been supported by the RF Ministry of Education and Science, Project RFMEFI57514X0003, by the State Program "Science", Project#533 and by TPU Grant IFVT_85_2014. The support of the San Diego State University researcher by the US Department of Energy, Materials Sciences Division, under Award No. DE-SC0008581 is gratefully acknowledged.

REFERENCES

1. V.A. Artemyev, *JTP Lett.* 23, 5 (1997).
2. I. Bogachev, E. Olevsky, E. Grigoryev, and O. Khasanov, *JOM* 66, 1020 (2014).
3. V.N. Gulbin, V.V. Polivkin, V.V. Cherdyntsev, M.V. Gorshenkov, RF Patent 2509818 (2014).
4. F. Muktepavela, I. Manika, and V. Mironov, *Mater. Des.* 18, 257 (1997).
5. V. Mironov, O. Filippov, and I. Boiko, *Eston J. Eng.* 16, 142 (2010).
6. M.S. Yurlova, V.D. Demenyuk, L.Y. Lebedeva, D.V. Dudina, E.G. Grigoryev, and E.A. Olevsky, *J. Mater. Sci.* 49, 952 (2014).
7. G. Lee, M.S. Yurlova, D. Giuntini, E.G. Grigoryev, O.L. Khasanov, J. McKittrick, and E.A. Olevsky, *Ceram. Int.* 41, 14973 (2015).
8. X. Wei, C. Back, O. Izhvanov, O.L. Khasanov, C.D. Haines, and E.A. Olevsky, *Materials* 8, 6043 (2015).
9. W. Li, E.A. Olevsky, O.L. Khasanov, C.A. Back, O. Izhvanov, J. Opperman, and H.E. Khalifa, *Ceram. Int.* 41, 3748 (2015).
10. E.G. Grigoryev, L.Y. Lebedeva, O.L. Khasanov, and E.A. Olevsky, *Adv. Eng. Mater.* 16, 792 (2014).
11. M.S. Yurlova, A.N. Novoselov, Y.S. Lin, O.N. Sizonenko, E.G. Grigoryev, O.L. Khasanov, and E.A. Olevsky, *Adv. Eng. Mater.* 16, 785 (2014).
12. A.V. Pustovalov and S.P. Zhuravkov, *Adv. Mater. Res.* 1097, 3 (2015).
13. S.J. Gregg and K.S.W. Sing, *Adsorption, Surface Area and Porosity*, 2nd ed. (Cambridge: Academic Press, 1982), p. 304.
14. T. Ichikawa, *Phys. Status Solidi A* 29, 293 (1975).
15. O.L. Khasanov and E.S. Dvilis, *J. Eur. Ceram. Soc.* 27, 749 (2007).
16. O.L. Khasanov and E.S. Dvilis, *Adv. App. Ceram.* 107, 135 (2008).
17. A.V. Kyulemin, *Metall. Mosc* 200 (1978).
18. E. Olevsky, *Mater. Sci. Eng. R* 23, 41 (1998).
19. W. Li, E.A. Olevsky, J. McKittrick, A.L. Maximenko, and R.M. German, *J. Mater. Sci.* 47, 7036 (2012).
20. Z.A. Munir, U. Anselmi-Tamburini, and M. Ohyanagi, *J. Mater. Sci.* 41, 763 (2006).
21. Z.A. Munir, D.V. Quach, and M. Ohyanagi, *J. Am. Ceram. Soc.* 94, 1 (2011).
22. R. Orru, R. Licheri, A.M. Locci, A. Cincotti, and G. Cao, *Mater. Sci. Eng. R* 63, 127 (2009).
23. S. Grasso, Y. Sakka, and G. Maizza, *Sci. Technol. Adv. Mater.* 10, 053001 (2009).